CONF-810406--4

MASTER

SOME FACTORS AFFECTING THE METERING OF SUBCOOLED WATER WITH A CHOKED VENTURI

James R. Fincke and David R. Collins

EG&G Idaho, Inc.
P.O. Box 1625
Idaho Falls, ID 83415

ABSTRACT

A series of experiments was performed to characterize the subcooled choking process in a convergent-divergent nozzle with a constant-area throat. The experiments were conducted in a low-pressure flow loop capable of a maximum water flow rate of 5.5 L/s with a pressure head of 300 kPa. The pressure and temperature upstream of the nozzle in the flow loop were adjusted between 90 and 300 kPa and 53 and 96°C, respectively. The variables measured in this study of critical flow phenomena were the flow rate, upstream pressure and temperature, and the axial wall pressure profiles in the nozzle. Critical mass flow rate data were acquired along five isotherms as a function of stagnation pressure. Factors affecting metering performance are examined.

INTRODUCTION

Accurate determination of the maximum discharge flow rate of a subcooled liquid from a nozzle is a problem which presents itself in the safety analysis of pressurized, water cooled nuclear reactors. The discharge flow rate is an important variable in these analyses because it affects the maximum core temperature and depressurization rate under loss-of-coolant accident conditions. This paper examines some of the factors affecting using a venturi to measure this discharge rate for subcooled upstream conditions. During flow rate experiments under typical reactor operating conditions, the subcooled liquid undergoes a partial phase change, resulting in a two-phase mixture in the venturi. Generally, when vapor is present in the venturi, the flow rate is at a maximum and dependent only upon upstream conditions; that is, the flow rate is independent of the downstream pressure.

The maximum flow rate of a fluid, generally referred to as choked flow or critical flow, is a well understood phenomena in gases. Experiments have shown that some similarities exist between critical two-phase flow and critical gas flow. As in gas flow for a given upstream pressure and temperature, a decrease in the downstream pressure keeps the two-phase flow rate unchanged, and thus at the maximum. In addition, all the flow parameters upstream of a fixed cross section remain unchanged.

In gas flows, an additional definition is often used: The flow is choked when the velocity at some cross section is equal to the velocity of sound at that point.

In two-phase flows, theoretical studies show that a relation between choked flow and sound velocity exists; however, this fact is difficult to verify experimentally. For this reason, the criteria used in this study to determine if a particular flow is choked are whether or not the flow rate and upstream conditions remain unchanged as the backpressure is varied.

An additional feature of critical two-phase flows is that the phase velocities at the critical flow condition can be much lower than the critical velocities of each phase considered separately. Thus, high velocities, or flow rates, are not necessarily associated with choked two-phase flow.

The results presented here are part of an experimental study undertaken to gain an understanding of the choking process in a convergent-divergent nozzle with a short, constant-area throat for subcooled upstream conditions. This type nozzle is commonly used in small scale loss-of-coolant experiments[1]. The choking process is characterized by nonequilibrium vapor generation and minimum static wall pressures in the throat which are less than the vapor pressure corresponding to the upstream temperature.

The following sections describe the test section and instrumentation and present results of the study including (a) single-phase data to characterize the single-phase nozzle performance, (b) the details of vapor generation or cavitation and some nonequilibrium effects, and (c) the details of the critical mass flow rate and nozzle discharge coefficient with special emphasis on the use of a venturi for metering subcooled fluids under choked conditions.

FLOW LOOP AND TEST SECTION

The flow loop is shown schematically in Figure 1. Tap water is circulated through 3-in. nominal diameter piping by a centrifugal pump at a flow rate of 5.5 L/s and at a head of 300 kPa. The tap water is degassed by heating to the boiling point;

DISCLAIMER

This book was prepared as an account of work sponsored by an agency of the United States Government. Neither the United States Government nor any agency thereof, nor any of their employees, makes any warranty, express or implied, or assumes any legal liability or responsibility for the accuracy, completeness, or usefulness of any information, apparatus, product, or process disclosed, or represents that its use would not infringe privately owned rights. Reference herein to any specific commercial product, process, or service by trade name, trademark, manufacturer, or otherwise, does not necessarily constitute or imply its endorsement, recommendation, or favoring by the United States Government or any agency thereof. The views and opinions of authors expressed herein do not necessarily state or reflect those of the United States Government or any agency thereof.

DISTRIBUTION OF THIS DOCUMENT IS UNLIMITED

the free surface in the calming tank is covered by a plastic film to prevent reabsorption of gas from the atmosphere.

In the direction of flow through the system, the main components are: the circulation pump, a flow control valve, a 3-in.-diameter turbine flow meter, the test section, a backpressure control valve, and the water supply tank containing an 8-kW heater. Hydraulically, the upstream pressure is set by the flow rate. The pump speed, controlled by a variable speed motor, was used to set the flow rate. The flow control valve immediately downstream of the pump was kept in the open position during the tests. The backpressure on the test system was adjusted by closing the backpressure control valve until the desired backpressure was obtained.

The advantage of operating the loop in this manner, rather than externally pressurizing the loop, is that better flow stability will result. In this mode, the flow is critical if the inlet pressure and flow rate remain constant with a change in downstream pressure. No flow limitations were observed in the loop, except those imposed by the pump.

The entire test section was fabricated from Lexan tubing so that visual observation of the flow phenomena can be made. The upstream run consists of a 1.8-m-long section of 4.34-cm-ID Lexan tubing; the length-to-diameter ratio is approximately 41. This should result in a fully developed turbulent flow field for the Reynolds number range tested, 10^5 to 10^6. The nozzle dimensions and pressure tap locations are shown in Figure 2. The pressure tap diameters are 0.76 mm. Care was taken to polish all inside surfaces to remove any burrs resulting from the fabrication process. During the polishing process, the throat entrance was slightly rounded. Despite the care taken in polishing, a few tool chatter marks remained at the diffuser entrance. The diffuser terminates in a constant-area downstream section that has a 3.49-cm ID and is 43 cm long, resulting in a length-to-diameter ratio of 12.

INSTRUMENTATION AND DATA ACQUISITION

The variables of interest in this study of initially subcooled choked flow are the flow rate, upstream temperature and pressure, and the axial static pressure profiles in the nozzle. The following discussion describes the experimental instrumentation used to provide these measurements and the data acquisition system used to obtain data for the study.

The flow rate was measured by a standard 3-in.-diameter ITT Barton flow meter, calibrated in the range of 0.3 to 10 L/s. The accuracy of this flow meter, obtained by calibration, is better than 1% of range.

The upstream temperature was measured in the 3-in. loop piping by a 1.45-mm-diameter, Type K, Chromel-Alumel sheathed, grounded junction thermocouple. The thermocouple was calibrated and found to read within $\pm 0.1^{\circ}C$ of standard Type K calibration values.

The upstream pressure was measured at the first nozzle pressure tap located upstream of the convergent section, Figure 2. The pressure transducers used for this measurement and the nozzle wall static pressure profile measurements were made with Validyne, Model DP15TL, differential pressure transducers. The accuracy of the pressure measurements, including pressure tap errors, was 1.4% of range. The pressure transducers were referenced to the atmosphere, a vacuum manifold, or a pressure manifold, as required. The pressures in the manifolds were adjusted, and transducer ranges picked, so that the respective pressures would fall in the upper 50% of the transducer range. The pressure in the manifolds was also measured by the Validyne pressure transducers referenced to the atmosphere. The local barometric pressure was obtained at the beginning of each test from a mercury barometer.

The portable data acquisition system, used for acquiring data in the experiments reported here, was constructed around a Hewlett-Packard 9825 programmable calculator and NEFF 620 front end. Data were typically acquired at a rate of 20 samples per second for a period of several seconds. Temporal averages and standard deviation were then computed. The sample period was chosen such that the temporal averages and standard deviations did not change with an increase in sample period.

AXIAL PRESSURE DISTRIBUTIONS FOR SINGLE-PHASE AND IDEAL ONE-DIMENSIONAL FLOW

A number of test points were taken to characterize the axial single-phase wall pressure distributions. Typical pressure drop results with respect to the upstream pressure as a function of axial distance are presented in Figure 3. The solid line on Figure 3 represents the ideal one-dimensional pressure distribution. The pressure coefficient, C_p, is defined as

$$C_p = \frac{P_o - P}{\frac{1}{2}\rho_l U_o^2}$$

where

P_o = stagnation pressure
P = static pressure
ρ_l = liquid density
U_o = upstream velocity.

In the converging section, the flow acceleration was accompanied by a pressure drop. The constant-area throat region exhibited evidence of strong two-dimensional effects shown by the deviation from the one-dimensional theory. The flow probably was separated in the near wall region due to the inability of the fluid to negotiate the relatively sharp corner. The deceleration in the diverging section resulted in the expected pressure recovery. The unrecovered pressure loss in the nozzle was due to friction losses.

CRITICAL MASS FLUX AND NOZZLE DISCHARGE COEFFICIENT

The critical mass flux taken along five different isotherms as a function of stagnation pressures is shown in Figure 4. As the stagnation pressure increased, the mass flux also increased. As the stagnation temperature increased, the critical mass flux decreased for a given stagnation pressure. The nozzle discharge coefficient, C, is defined by

$$C = \frac{G^*}{[2\,\rho_l\,(P_o - P^*)]^{1/2}}$$

where

G^* = mass flux in the throat
ρ_l = liquid density
P^* = throat pressure.

In determining the discharge coefficient, two major approaches have traditionally been used: The first is to actually measure the difference between the throat pressure and stagnation pressure; the second is to assume that throat pressure is equal to the vapor pressure corresponding to the upstream temperature. As shown in a later section, the second approach is generally not satisfactory. In addition, the appearance and configuration of the vapor (cavitation regime) in the venturi can effect the discharge coefficient; this effect is discussed in the following section.

The nozzle discharge coefficient, exclusive of cavitation regime and nonequilibrium effects, is shown in Figure 5 as a function of Reynolds number. There appears to be no systematic variation with Reynolds number or temperature over the limited range of this study. The scatter in the data is typical, the uncertainty in the discharge coefficient is 2%.

CAVITATION REGIME EFFECTS

Several cavitation regimes were observed during testing, and their existence was recorded photographically. The cavitation regimes are important because they effect nozzle performance. In this section, the cavitation regimes observed during testing are discussed, and the effect on discharge coefficient is presented.

Figure 6 shows cavitation inception on the throat pressure taps. The phenomena of cavitation inception on isolated surface irregularities is well known[2,3], and indeed, it is on these irregularities that vapor generation was first observed in the nozzle tested here. The flow in this case was not choked; this was verified by raising the backpressure and observing that the upstream pressure was also affected.

As the flow rate was increased, the flow regime pictured in Figure 7 appeared. This flow condition, characterized by a large vapor plume initiated by the presence of the pressure taps and a condensation zone downstream of the throat, was found to be stable and choked. As the flow rate was further increased, the flow regime pictured in Figure 8 appeared. This flow condition was characterized by a liquid core surrounded by a vapor annulus. This flow regime was also stable and choked and, in addition, was found to persist as the flow rate was decreased. Thus, for the same flow rate, it is possible for two regimes to exist, depending on the direction from which the flow condition is approached. Flow hysteresis is well known in both cavitating and noncavitating systems, and it is not surprising that the phenomenon appears here. Figure 9 presents a comparison of the axial pressure profiles for the two regimes. The profiles are quite similar, with the major deviations occurring in the condensation region. One should also note that the pressure in the region between the throat entrance and the condensation region is relatively constant, and that pressure recovery and the condensation region are coincident.

As the flow rate was even further increased, a third regime (Figure 10) characterized by delayed vapor generation appeared. In this flow regime, little vapor appeared in the throat, primarily streaming off surface irregularities. The fluid residence time in the throat (< 1 ms) was so short that the fluid did not have sufficient time to change phases. The major generation of vapor appeared at the diffuser entrance and in the diffuser itself. It was found that this third flow regime was stable and did not coexist with any other regime.

The discharge coefficient exhibited some dependence on the cavitation regime, as shown in Figure 11. The major effect appeared for the cavitation regime, characterized by a vapor plume initiated at the pressure taps. This cavitation regime displayed a slightly higher discharge coefficient which probably resulted from an effective increase in throat area due to less vapor generation. As the Reynolds number was increased, uniform cavitation was established and the separated region in the throat attained a limiting form, not dependent upon the presence of liquid or vapor.

NONEQUILIBRIUM EFFECTS

The isothermal expansion of a liquid may be represented in the P-T plane by a vertical line, Figure 12. Point A defines the nozzle inlet condition (P_o,T_o), and Point B, the condition at the throat. The distance A-B is related to the mass flux through the nozzle. For a given inlet condition, the saturation line may be crossed in the expansion for some values of mass flux. If the mixture were in equilibrium and two-dimensional effects were negligible, the throat pressure B would be equal to the vapor pressure. In real nozzles, however, minimum pressures less than the vapor pressure are routinely observed; furthermore, the *minimum* pressure is not a simple function of upstream conditions. The result is a vapor-liquid mixture which is not in equilibrium. It is these nonequilibrium effects and the vapor cavity configuration that strongly influence the maximum discharge rate through a nozzle.

Figure 13 shows the difference between P_v (the vapor pressure corresponding to the upstream temperature) and P* (the throat pressure non-dimensionalized by the kinetic energy of the flow), assuming all liquid was one-dimensional flow in the throat, plotted against the Reynolds number based on throat diameter for a constant stagnation temperature of 75°C. The cavitation regime effect was obvious, with an apparent higher degree of pressure nonequilibrium existing for the cavitation plume initiated by the pressure taps. This was probably due to less interfacial area available for heat transfer. Thus, for the same upstream flow rate, the throat pressure was not necessarily unique. In addition, the pressure nonequilibrium was not a simple function of the upstream conditions. Further investigation[4] of this phenomena has shown that both thermodynamic effects and the turbulent transport of thermal energy play an important role in determining the nonequilibria in the venturi. For systems in which the vapor pressure, corresponding to the upstream temperature, is of the same order of magnitude as the upstream pressure, it is not sufficient to assume that the throat pressure is equal to this vapor pressure. As the upstream temperature increases, the effect becomes larger. Therefore, the difference in the throat pressure and stagnation pressure must be measured directly to assure accurate flow measurement.

CONCLUSIONS

In this paper, experimental results are presented which in part characterize the choking process in a convergent-divergent nozzle with a constant-area throat for subcooled upstream conditions. The converging-diverging nozzle was found to behave somewhat differently from the performance predicted by the ideal one-dimensional theory. The differences are not explainable by friction effects alone. The data indicate that the flow field was strongly two-dimensional in the throat region.

The critical mass flow rate was found to be a function of both upstream pressure and upstream temperature, with the mass flow rate increasing with pressure and decreasing with temperature. The nozzle discharge coefficient was found to be constant over the range tested, once fully developed cavitation was established.

Once the nozzle flow rate was high enough to choke the flow, the factors that affected the maximum discharge rate were stagnation pressure, stagnation temperature, and cavitation regime. The cavitation regime depended on the direction from which the flow condition was approached and the presence of throat pressure taps and isolated surface irregularities. To minimize this affect, the throat pressure tap should be as small as possible and the entire nozzle inside finish free from burrs. It is not sufficient to infer the throat pressure from the vapor pressure corresponding to the upstream temperature. The difference between the throat pressure and upstream pressure must be measured directly.

REFERENCES

(1) Hanson, Robert G., Evaluation of the Effects of Break Nozzle Configuration in the Semiscale MOD-1 System, TREE-NUREG-1118, EG&G Idaho, Inc., August 1977.

(2) Arndt, R. E. and Ippen, A. T., "Rough Surface Effects on Cavitation Inception," Journal of Basic Engineering, Transactions of the ASME, June 1978.

(3) Holl, J. W., "The Inception of Cavitation on Isolated Surface Irregularities," Journal of Basic Engineering, Transactions of the ASME, March 1960.

(4) Fincke, James R., The Correlation of Two-Dimensional and Nonequilibrium Effects in Subcooled Choked Nozzle Flow, EG&G Idaho, Inc., to be published.

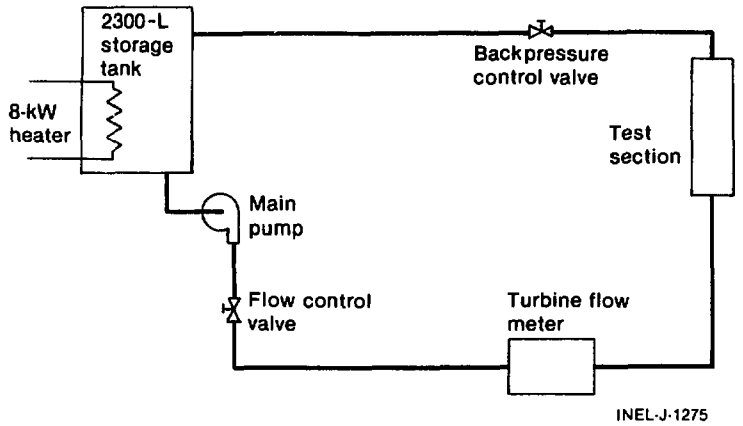

Figure 1. Schematic of Flow Loop.

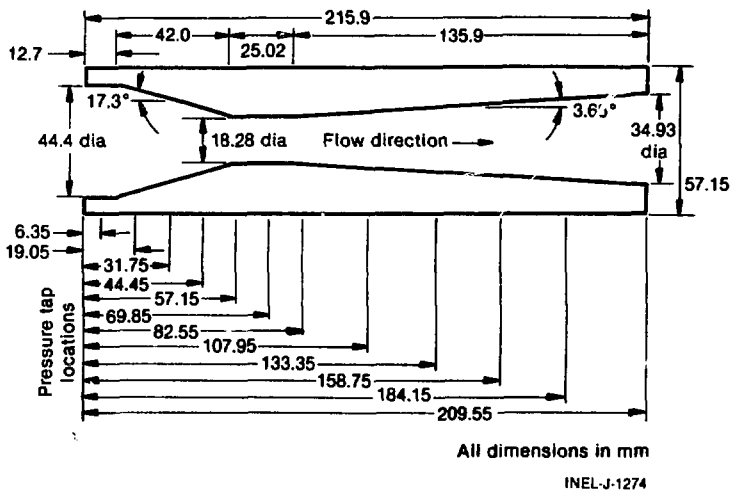

Figure 2. Convergent-Divergent Nozzle Geometry.

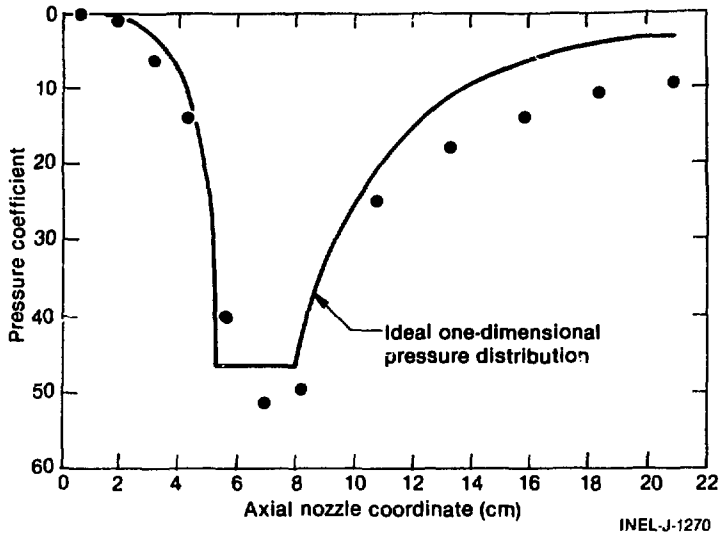

Figure 3. Single-Phase Axial Pressure Distribution.

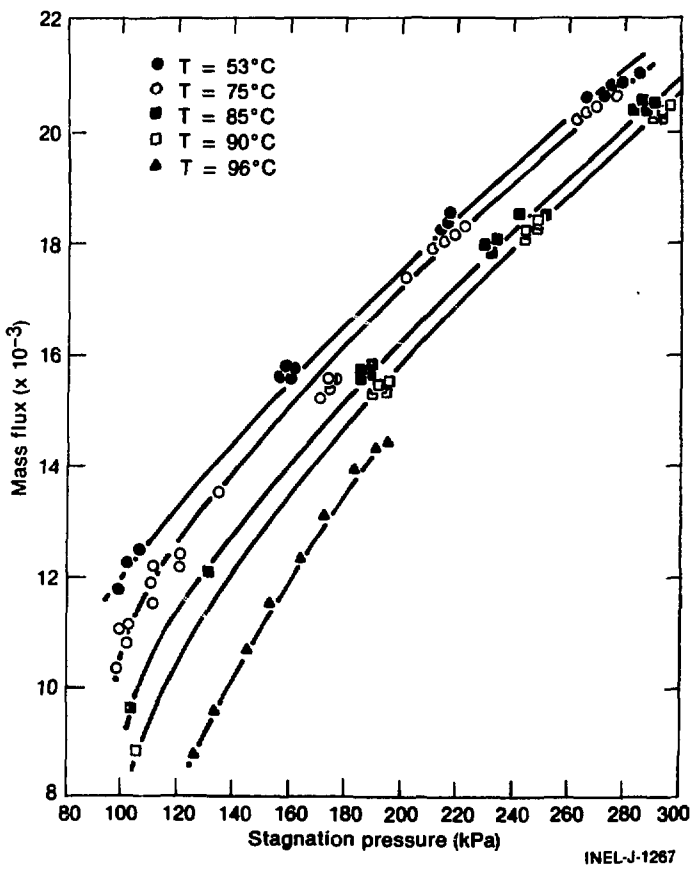

Figure 4. Mass Flux as a Function of Stagnation Pressure for Five Isotherms.

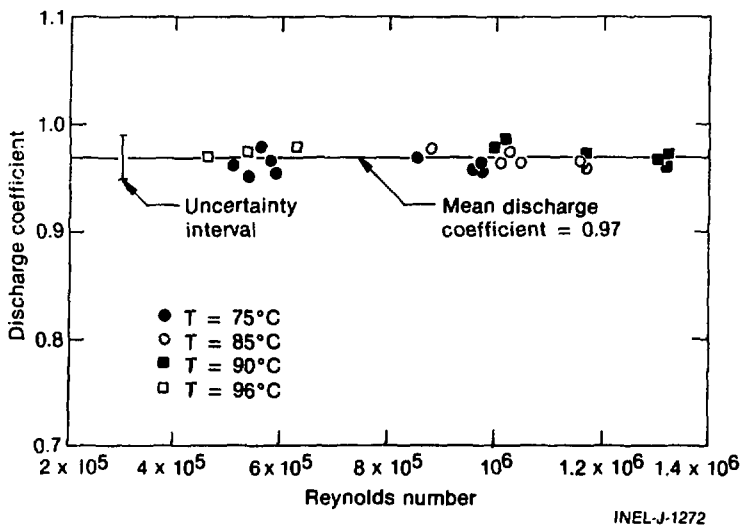

Figure 5. Nozzle Discharge Coefficient, Irrespective of Cavitation Regime Effects.

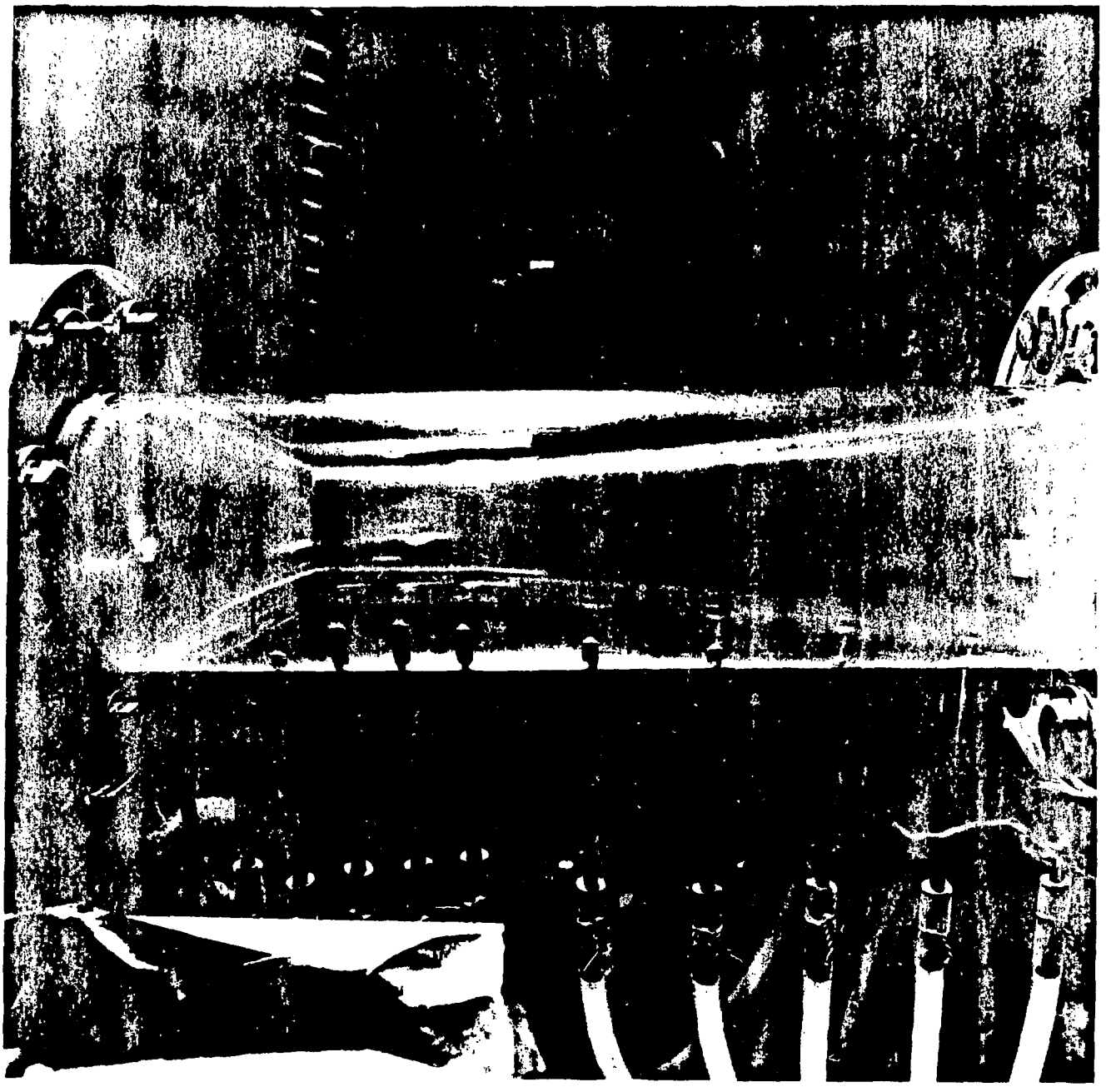

Figure 6. Cavitation Inception on Throat Pressure Taps.

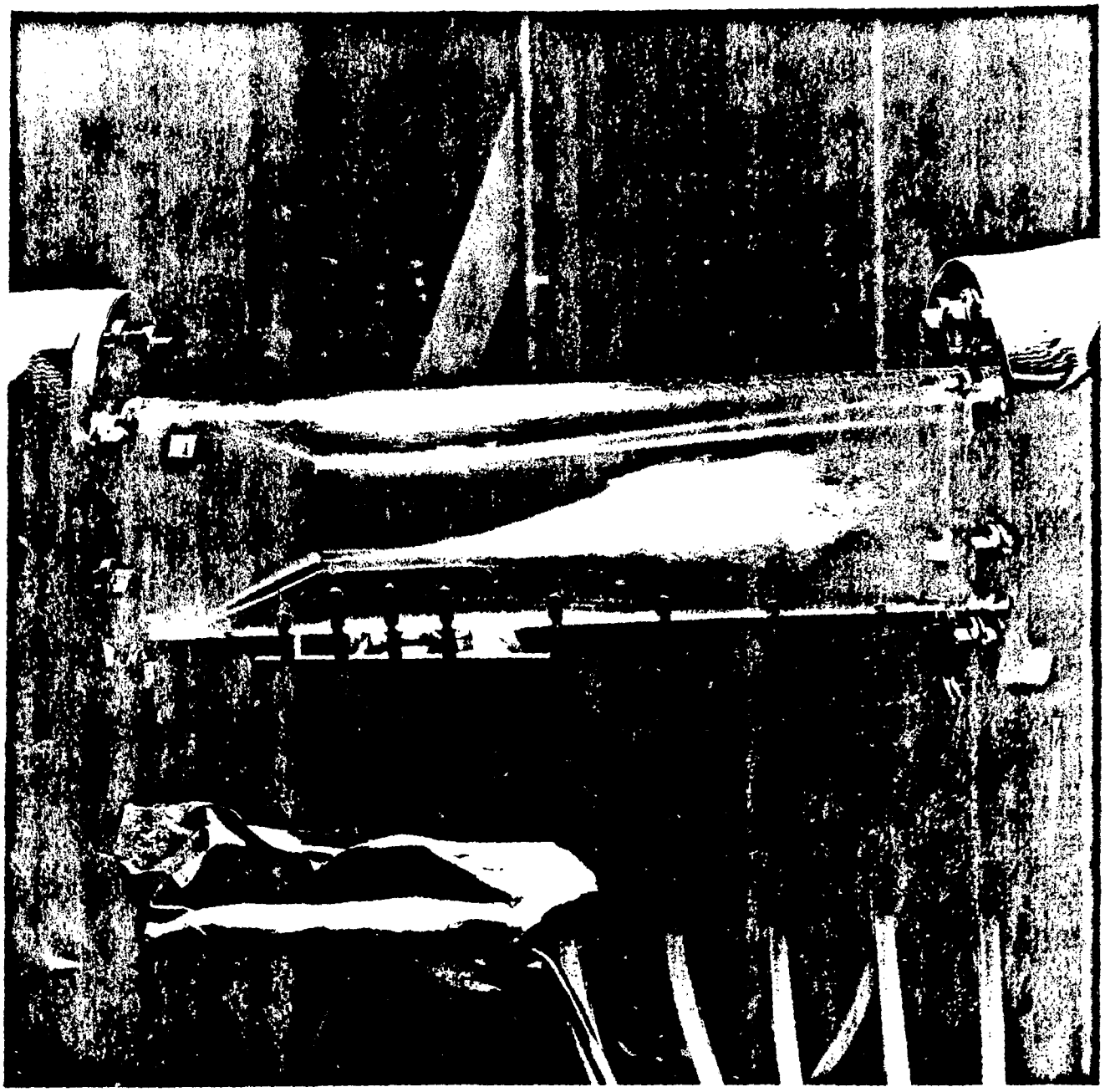

Figure 7. Vapor Plume Initiated by Throat Pressure Taps.

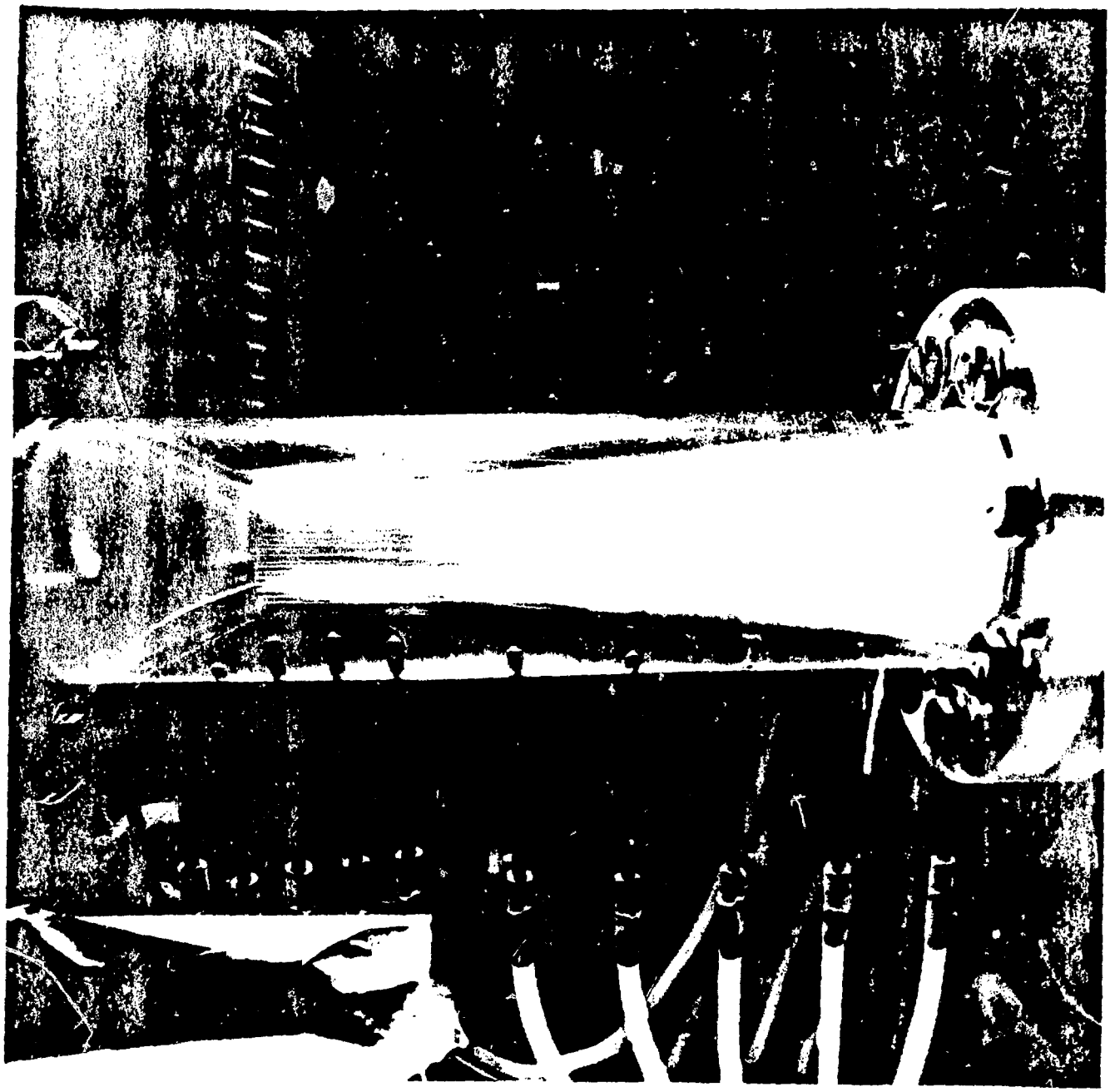

Figure 8. Inverted Annular Cavitation.

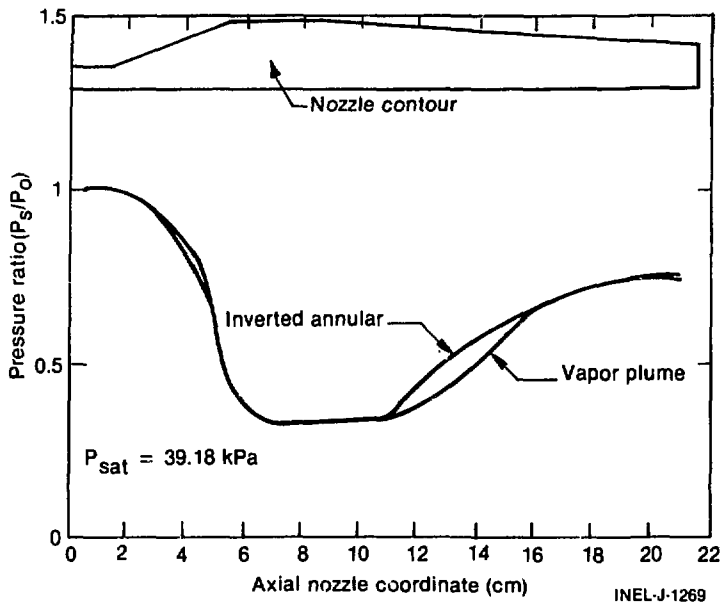

Figure 9. Comparison Between Axial Pressure Profiles for Vapor Plume and Inverted Annular Cavitation Regimes.

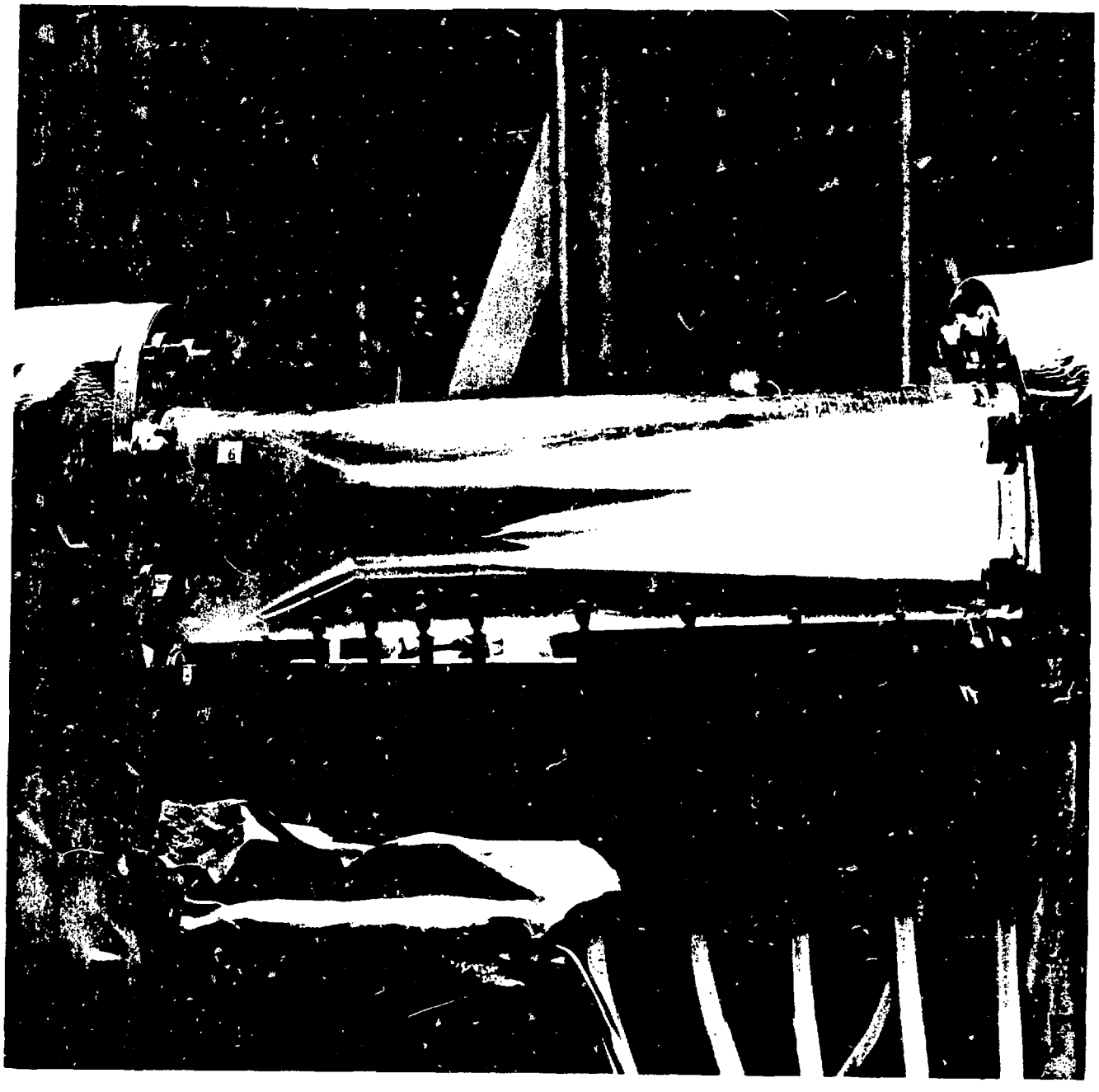

Figure 10. Cavitation Regime Characterized by Delayed Vapor Generation.

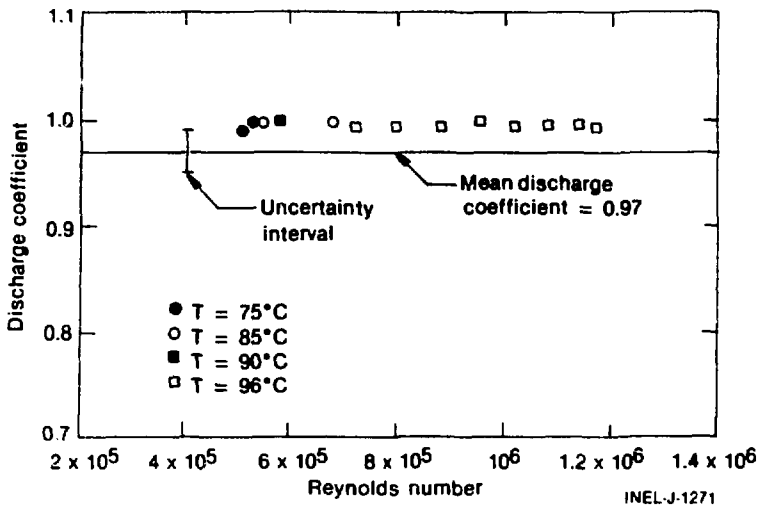

Figure 11. Nozzle Discharge Coefficient Displaying Cavitation Regime Effects.

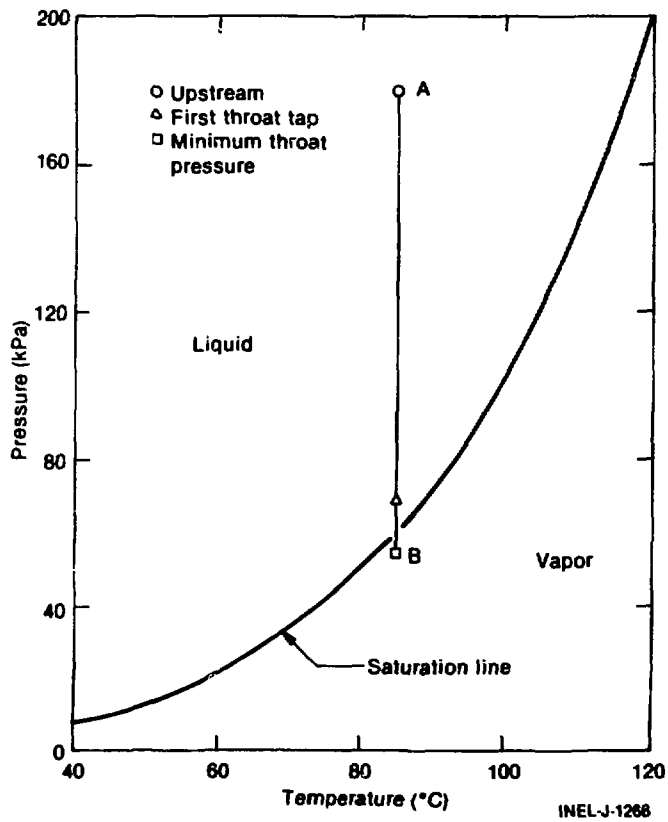

Figure 12. Typical Representation of Isothermal Flashing on the Pressure-Temperature Diagram.

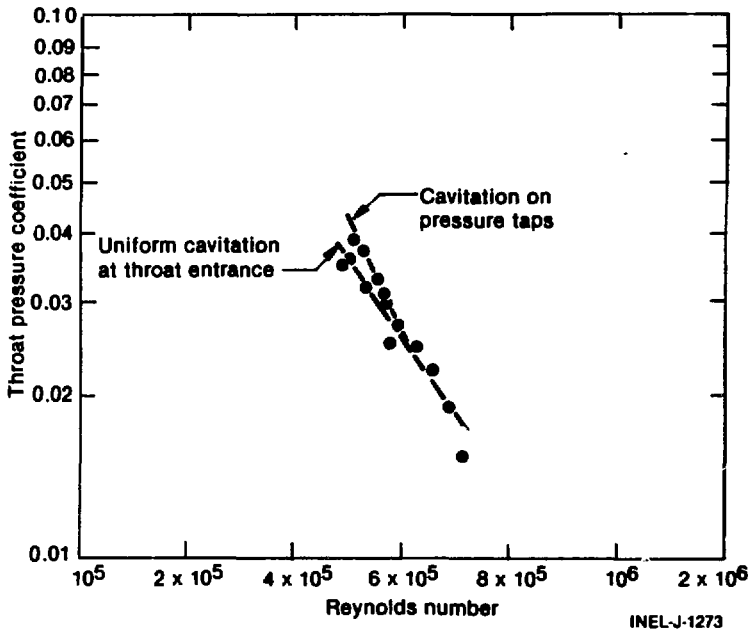

Figure 13. Throat Pressure Coefficient versus Reynolds Number for Vapor Plume and Inverted Annular Cavitation Regimes.